From quasi-two-dimensional metal with ferromagnetic bilayers to Mott insulator with G-type antiferromagnetic order in Ca_{3}(Ru_{1−x}Ti_{x})_{2}O_{7}

Jin Peng, X. Ke, Gaochao Wang, J. E. Ortmann, David Fobes, Tao Hong, Wei Tian, Xiaoshan Wu, and Z. Q. Mao

Phys. Rev. B **87**, 085125 — Published 20 February 2013

DOI: 10.1103/PhysRevB.87.085125

From quasi-2D metal with ferromagnetic bilayers to Mott insulator with G-type antiferromagnetic order in $Ca_3(Ru_{1-x}Ti_x)_2O_7$

Jin Peng,[1] X. Ke,[2,3] Gaochao Wang,[1] J. E. Ortmann,[1] David Fobes,[1] Tao Hong,[2] Wei Tian,[2] Xiaoshan Wu,[4] and Z. Q. Mao[1,*]

[1]*Department of Physics and Engineering Physics, Tulane University, New Orleans, Louisiana 70118, USA*
[2] *Quantum Condensed Matter Division, Oak Ridge National Laboratory, Oak Ridge, Tennessee 37831, USA*
[3]*Department of Physics and Astronomy, Michigan State University, East Lansing, MI 48825, USA*
[4]*Department of Physics, Laboratory of Solid State Microstructures, Nanjing University, Nanjing 210093, China*

(Dated: December 21, 2012)

We report the electronic and magnetic phase diagram of $Ca_3(Ru_{1-x}Ti_x)_2O_7$. With Ti doping, the system evolves from a quasi-2D metal with ferromagnetic (FM) bilayers coupled antiferromagnetically along the c-axis (AFM-b) for $x = 0$, to a weakly localized state for $0 < x < 0.05$ and finally to a Mott insulator with G-type antiferromagnetic (G-AFM) order for $x \geq 0.05$. The magnetic state switching from the AFM-b to the G-AFM occurs in the weakly localized state near $x = 0.03$. We show that such a magnetic transition is controlled by the charge carrier itinerancy and can be understood in light of competing interactions between FM double-exchange and AFM superexchange. An incommensurate component is also observed due to competing magnetic interactions.

PACS numbers: 77.80.bj,74.70.Pq,71.27.+a

I. INTRODUCTION

There has been intensive research on strongly correlated transition metal oxides (TMOs) in past decades since they display a broad range of fascinating phenomena, such as high-T_c superconductivity and colossal magnetoresistance (CMR). In general, TMOs possess several simultaneously active degrees of freedom involving charge, spin, lattice and orbital. The complex interplay of these degrees of freedom results in a soft electronic state that can be easily modified by external perturbations.[1] Ruddlesden-Popper (RP) type layered ruthenates, $(Sr,Ca)_{n+1}Ru_nO_{3n+1}$,[2] are typical correlated materials, which have attracted widespread attentions. The properties of ruthenates can be easily tuned by dimensionality, magnetic field or chemical doping. For examples, in $Sr_{n+1}Ru_nO_{3n+1}$, with an increase of RuO_2 layer number n, the system evolves from spin-triplet superconductor Sr_2RuO_4 ($n = 1$)[3–5] to strongly enhanced paramagnetic $Sr_3Ru_2O_7$ ($n = 2$) with a field tuned nematic phase[6–9] and finally to itinerant ferromagnetic (FM) $SrRuO_3$ ($n = \infty$).[10] In single layered ruthenates $Ca_{2-x}Sr_xRuO_4$, with Ca substitution for Sr, the system is successively driven from a superconducting state to a nearly FM metal, and finally to an antiferromagnetic (AFM) Mott insulator ($x < 0.2$).[11–14]

This paper focuses on Ti doping effect in $Ca_3Ru_2O_7$. Undoped $Ca_3Ru_2O_7$ orders antiferromagnetically at $T_N = 56$ K,[15] with FM bilayers antiferromagnetically coupled along the c-axis.[16,17] The AFM transition is closely followed by a first-order metal-insulator transition (MIT) at $T_{MIT} = 48$ K,[15] with a quasi-2D metallic state for $T < 30$ K.[18] Photoconductivity[19] and Raman spectroscopy[20] measurements reveal the MIT to be associated with the opening of a charge gap and suggest orbital ordering. Angle-resolved photoemission spectroscopy measurements[21] further show that while large portions of the Fermi surface are indeed gapped below T_{MIT}, some small metallic, non-nested pockets survive. Moreover, $Ca_3Ru_2O_7$ exhibits giant magnetoresistance associated with a bulk spin valve effect.[16,17,22,23] These rich properties imply competing physical interactions of comparable strength between spin, charge, lattice, and orbital degrees of freedom in $Ca_3Ru_2O_7$. Therefore, $Ca_3Ru_2O_7$ is expected to be sensitive to external stimuli.

Our earlier work has revealed that Ti doping into Ru sites can turn the system to a Mott insulating state with G-type AFM order.[24] In this paper, we report the electronic and magnetic phase diagram of this doped system and discuss the mechanism for the magnetic and Mott transitions. We find that the magnetic transition from intralayer FM coupling to the nearest-neighbor AFM coupling occurs in a weakly localized state near $x = 0.03$, while the Mott transition does not occur until x is increased above 0.05. Our analyses show that the itinerancy of charge carriers is extremely sensitive to Ti doping and that the decrease of itinerancy induced by doping plays a pivotal role in driving the magnetic transition.

II. EXPERIMENT

Single crystals of $Ca_3(Ru_{1-x}Ti_x)_2O_7$ used in this study were grown by floating zone technique. All samples used in the experiment were examined by X-ray diffraction (XRD) measurements and were shown to be composed of pure

bilayered phase. The resistivity and specific heat of the samples were measured with a four-probe method and an adiabatic relaxation technique, respectively, in a physical property measurement system (PPMS, Quantum Design). Magnetization measurements were performed with a superconducting quantum interference device (SQUID, Quantum Design) magnetometer. We also performed neutron scattering measurements on several typical samples using HB1A thermal neutron triple-axis spectrometers at Oak Ridge National Laboratory. Detailed neutron experiment setup has been described in the earlier work.[24]

III. RESULTS AND DISCUSSIONS

The phase diagram of electronic and magnetic properties for $Ca_3(Ru_{1-x}Ti_x)_2O_7$ is presented in Fig.1(a). We observe several distinct ordered magnetic phases in the phase diagram. For the end member ($x = 0$), it first shows an AFM transition at 56 K, then followed by a MIT at 48 K, as noted above. This AFM state is characterized by FM bilayers coupled antiferromagnetically along the c axis and the spin direction switches from the a-axis for $T_{MIT} < T < T_N$ to the b-axis for $T < T_{MIT}$ (see Fig. 1b).[16] We name these two magnetic states as AFM-a and AFM-b, respectivity, following the notations used in ref. 16. For $x \geq 0.03$, the magnetic state changes to a G-type antiferromagnetically ordered state[24] and the magnetic transition merges with the MIT as x is increased above 0.04. As shown in Fig. 1(b), the G-type AFM state is characterized by nearest-neighbor AFM coupling for both in-plane and the c-axis directions, in sharp contrast with the FM coupling within bilayer in the AFM-a or AFM-b state. When $x > 0.15$, the magnetic/MI transition is smeared out. For $0 < x \leq 0.03$, the system shows complex magnetic transitions. We find an intermediate magnetic (IM) phase in a narrow temperature range between AFM-a and AFM-b, which shows an incommensurate component. While the AFM-a phase exhibits metallic behavior, the AFM-b phase for $0 < x \leq 0.03$ displays weakly localized electronic state, in contrast with the quasi-2D metallic ground state of $Ca_3Ru_2O_7$. The weakly localized state extends across the AFM-b/G-AFM boundary and switches to the Mott insulating state for $x \geq 0.05$.

The phase diagram described above was established by systematic measurements of neutron scattering, resistivity, magnetization and specific heat. The magnetic transitions probed by these various techniques are consistent with one another. The magnetic structures of the AFM-a/b and G-AFM phases were determined in our previous work using the $x = 0$ and 0.03 samples.[16,24] In order to map out the complete magnetic phase boundaries, we have performed further neutron scattering measurements on the samples with $x = 0.02$, 0.03 and 0.1. Fig. 2a presents the temperature dependence of the neutron scattering intensity of the (102) magnetic Bragg peak for the $x = 0.1$ sample, which indicate it possesses the G-AFM magnetic states below T_N.[24] A steep magnetic transition at 113 K can be seen clearly. This magnetic transiton happens simultaneously with a first-order structural transition. This structural transition does not involve a symmetry change, with the space group remaining in $Bb2_1m$ across the transition; however, the lattice parameters exhibit remarkable changes at the transition, with $\Delta a/a \sim 0.05\%$, $\Delta b/b \sim 1.0\%$ and $\Delta c/c \sim$ -0.84%.

The $x = 0.03$ sample exhibits complex magnetic transitions. It first displays the AFM-a order below 65 K, and then evolves into the G-AFM order below $T_{MIT} = 46$ K.[24] Our current systematic measurements revealed that the transformation from the AFM-a to the G-AFM occurs within a narrow temperature range (40 K - 44 K) where the IM phase is present. As shown in Fig. 2b and 2c, there exists three magnetic phases in this temperature region. From the (H 0 5) scans at various temperatures in Fig. 2b, we can see that as temperature is lowered below 46 K, the (005) magnetic peak, which corresponds to the AFM-a order, is dramatically suppressed and that weak incommensurate peaks develop simultaneously, with an incommensurate wave vector ($\pm\delta$ 0 5) where $\delta = 0.022 \pm 0.002$. In addition to the incommensurate component, a strong G-AFM component at (102) develops, which is revealed by the (H 0 2) scans (Fig. 2c). Below 40 K, the incommensurate component vanishes and the weakened AFM-a component transforms into AFM-b though its volume fraction is extremely small. The G-AFM order survives as a major phase. These three magnetic components in the 40 - 44 K range may imply a unique magnetic phase separation.

Complex magnetic transitions for $0 < x \leq 0.03$ range were also revealed in magnetic susceptibility and specific heat measurements. We present the data for the $x = 0.02$ sample in Fig. 3 where the $x = 0.1$ sample is also included for comparison. Apparently there exists an intermediate phase (represented by the purple color) between $T' = 43$ K and $T_{MIT} = 45.5$ K for the $x = 0.02$ sample, a feature similar to that seen in the $x = 0.03$ sample.[24] From the preliminary neutron scattering measurements (data not shown here), we found that this sample exhibits the AFM-a order for $T_{MIT} < T < T_N$, but the AFM-b order for $T < T'$. Further measurements are needed to identify the components of the IM phase in this sample. In contrast, the IM phase was not observed in the $x = 0.1$ sample (see Fig. 3c and 3d).

The electronic properties of the various magnetic states described above were examined by in-plane resistivity ρ_{ab} measurements. As shown in Fig. 4, the magnetic states of AFM-a, AFM-b and G-AFM are characterized by distinct electronic properties. For pure $Ca_3Ru_2O_7$, previous work has shown that the AFM-a phase for $T_{MIT} < T < T_N$ is metallic, while the AFM-b phase first displays insulating-like behavior in a temperature range immediately below T_{MIT}, then followed by quasi-2D metallic behavior for $T < 30$ K.[18] The AFM-a phase for $0 < x \leq 0.03$ maintains

metallic properties; however, the AFM-b or G-AFM phase in this range exhibits weak localization behavior, which is manifested in the observation that while the temperature dependence of ρ_{ab} becomes non-metallic (see Fig. 4a), the electronic specific heat coefficient γ_e is noticeably enhanced (see below). For the G-AFM state with $x \geq 0.05$, ρ_{ab} increases by 7-8 orders of magnitude, indicating a truly insulating state (see Fig. 4b).

The phase diagram established above reveals a challenging question: Why the Mott insulating state with the G-AFM order is so close to a quasi-2D metal with FM bilayers though they are seemingly energetically far from each other? In general, Mott transition can be approached by either band-filling control (*e.g.* in high-T_C cuprate and CMR manganite systems) or the band-width control (*e.g.* in $Ca_xSr_{2-x}RuO_4$). Although a similar magnetic transition from quasi-2D FM to the G-AFM order was previously reported in bilayered manganites,[25] as much as 70% hole doping is required to drive this transition and this transition occurs via several intermediate magnetic states. Since Ti and Ru have the same chemical valence, *i.e.* +4, Ti doping into Ru sites in $Ca_3Ru_2O_7$ should not introduce any additional charge carriers. As a result, the Mott transition tuned by Ti doping should not be associated with the band-filling control mechanism.

Band-width tuned Mott transitions usually take place via the $GdFeO_3$-type structural distortion which involves octahedral rotation and tilting. The Mott transition in $Ca_{2-x}Sr_xRuO_4$ represents a typical example for this scenario.[11–14] To examine if the Mott transition caused by Ti doping in $Ca_3Ru_2O_7$ is associated with the band-width tuning, we analyzed how Ti-doping affects the structure through structure refinements of XRD spectra at room temperature. We find that Ti-doping weakens the structural distortion, *i.e.* RuO_6 octahedral rotation and tilting angles (ϕ, θ) decrease strikingly with an increase of Ti content, as shown in Fig. 5a. The orthorhombicity reduces accordingly, due to the weakened structural distortion, as seen in the variation of lattice parameters in Fig. 5b. Such structural variation appears to widen the conduction bands. However, the density function theory (DFT) calculations indicated that the Ti t_{2g} band is above the Fermi level, hardly having contribution to Fermi surface. This implies that charge carriers cannot hop through Ti sites. That is, Ti impurities act as strong scattering centers, which naturally results in band narrowing as revealed by the DFT calculations.[24] The Mott transition near $x = 0.05$ is most likely associated with such a unique band narrowing effect.[24]

Another noteworthy question shown in the phase diagram is why the AFM-b-to-G-AFM magnetic transition takes place in the localized state near $x = 0.03$, rather than simultaneously with the Mott transition near $x \sim 0.05$. The most possible origin of such inconsistent electronic and magnetic transitions may be attributed to the phase separation caused by chemical inhomogeneity. In general, chemical inhomogeneity is unavoidable for any doped systems. The results of neutron scattering measurements on the $x = 0.03$ sample presented above actually reflects the existence of magnetic phase separation. Specially, although the system is dominated by the G-AFM phase in the ground state for 3% Ti doping, a minor AFM-b phase exists due to Ti-deficiency in some local areas. The AFM-b domains should have Ti concentration < 3% according to the phase diagram in Fig. 1. Since the AFM-b phase exhibits weak localization behavior in electronic transport and has resistivity much smaller than that of the insulating, G-AFM phase, the system is expected to show transport properties of weak localization when the minor AFM-b phase forms a percolative network in the G-AFM background. As Ti content further increases, we can imagine that the number of Ti-deficient domains (< 3% Ti) would becomes less. The weak localization behavior in transport should disappear when Ti concentration is high enough to break the percolative network of the AFM-b phase. From the phase diagram in Fig. 1, the critical Ti concentration for the disappearance of the electronic percolative effect appears to be $\sim$ 5%.

Such a picture of electronic percolation near the AFM-b/G-AFM magnetic phase boundary is strongly supported by the results of our specific heat measurements. Figure 6a and 6b show the low-temperature specific heat data of the samples with various Ti contents. For the undoped sample $Ca_3Ru_2O_7$, the specific heat divided by the temperature C/T exhibits T^2 dependence in the 2 - 8 K temperature range. The electronic specific coefficient γ_e obtained by fitting the data to $C = \gamma_e T + \beta T^3$ (where $\gamma_e T$ and βT^3 represent electronic and phonon specific heat respectively) is $\sim$ 1.84 mJ/(Ru mol K^2). This small value of γ_e is consistent with the previously reported value ($\sim$ 1.7 mJ/(Ru mol K^2)) for floating-zone grown single crystals[18] and should be attributed to the non-nested small Fermi pockets surviving from the MIT.[23] However, the samples doped with 1% and 2% Ti exhibit distinct behavior in comparison with $Ca_3Ru_2O_7$. Their specific heat values are much greater. Their C/T vs T^2 plots deviate from linearity and exhibit slight downward curvature, which suggests remarkable changes of electronic states and/or the presence of magnetic contribution. Since the magnetic structure of the AFM-b phase is analogous to the A-type AFM order (*i.e.* FM sheets stacked antiferromagnetically along the *c*-axis), we assume that the magnon contribution to the specific heat for the AFM-b phase is similar to that for the A-type AFM phase observed in $LaMnO_{3+\delta}$[26], *i.e.* $C_m \propto T^2$. As shown in Fig. 6a, the specific heat data of both samples can be best fitted to $C = \gamma_e T + BT^2 + \beta T^3$ where BT^2 stands for the magnetic contribution. The γ_e values obtained from these fittings are 10.9 mJ/(Ru mol K^2) and 8.9 mJ/(Ru mol K^2), respectively for 1% and 2% Ti doping, much greater than that of $Ca_3Ru_2O_7$. We did a similar fitting using $C = \gamma_e T + BT^2 + \beta T^3$ for $Ca_3Ru_2O_7$. The obtained γ_e is nearly the same as the value derived from the fitting without considering the magnetic contribution. This implies that the magnetic contribution is nearly negligible for $Ca_3Ru_2O_7$ for $T > 2.2$ K.

For the $x \geq 0.03$ samples with the G-AFM ground state, their specific heat values are much less than those of the $x = 0.01$ and 0.02 samples, but comparable to that of $Ca_3Ru_2O_7$ (see Fig. 6b). The magnon contribution to the specific heat for a G-AFM state is generally expected to show T^3 dependence;[26] hence it is difficult to separate it from the phonon contribution. The specific heat data for the samples with $x = 0.03$, 0.04, 0.05, 0.1 and 0.12 can all be fitted with $C = \gamma_e T + \beta T^3$. The botained γ_e values are presented in the inset of Fig. 6b where the γ_e values of the $x = 0$, 0.01 and 0.02 samples are also given for comparison. γ_e shows an interesting variation with Ti concentration: γ_e is ~ 1.84 mJ/(Ru mol K^2) for $Ca_3Ru_2O_7$, rises to ~ 10 mJ/(Ru mol K^2) for $x = 0.01$ - 0.02, then drops to ~ 1 mJ/(Ru mol K^2) for $x = 0.03$ - 0.04 and finally down to 0.5 mJ/(Ru mol K^2) for $x \geq 0.05$. In general, γ_e should be zero for a typical Mott insulating state. However, those $x \geq 0.05$ samples with insulating behavior in electronic transport show small γ_e values (~ 0.5 mJ/(Ru mol K^2)). This can be well understood in term of the phase separation caused by chemical inhomogeneity discussed above. In other words, due to the inhomogeneous distribution of Ti, some local areas may have Ti concentration less than 3%, resulting in some AFM-b domains embedded in the G-AFM matrix. These Ti-deficient, AFM-b domains should have tiny volume fraction since they are not sufficient to generate an electronic percolation effect in transport. Since the AFM-b phase is characterized by weakly localized states as discussed above, the AFM-b domains should be responsible for the small γ_e value. The relatively larger γ_e values (~ 1 mJ/(Ru mol K^2)) observed in the $x = 0.03$ and 0.04 samples agrees well with the chemical inhomogeneity interpretation for non-zero γ_e in the Mott insulating state for $x \geq 0.05$. As indicated above, these two samples exhibit weakly localized behavior in transport despite possessing the G-AFM ground state. Their larger γ_e values imply that the volume fraction of the minor AFM-b phase in these two samples is greater than that in those $x \geq 0.05$ samples. This is in line with the electronic percolation effect proposed above for these two samples. Such non-zero γ_e in an insulating state due to phase separation is often observed near the doping-induced MIT of TMOs, *e.g.* in $La_{1-x}Sr_xCoO_3$.[27]

Next, we will discuss why the $x = 0.01$ and 0.02 samples exhibit large γ_e values (~ 10 mJ/(Ru mol K^2)). In general, large γ_e is not expected for the insulating state near a MIT. However, the doped $Ca_3Ru_2O_7$ appears to be an exceptional case. As stated above, while large portions of the Fermi surface in $Ca_3Ru_2O_7$ are gapped as the temperature is lowered below $T_{\rm MIT}$ (= 48 K), some small metallic, non nested pockets survive. The electronic states from these small Fermi pockets become coherent only at low temperatures, which is responsible for the quasi-2D metallic behavior observed in electronic transport below 30 K.[18] These weakly coherent electronic states are susceptible to disorder scattering. For instance, in $(Ca_{1-x}Sr_x)_3Ru_2O_7$, we found that with partial Sr substitution for Ca ($x < 0.4$),[28] the electronic ground state transforms from a quasi-2D metallic state for $Ca_3Ru_2O_7$ ($x = 0$) to an Anderson localized state for $0 < x < 0.4$ and this localized state is attributed to disorder scattering induced by chemical substitution. An increase of γ_e is also observed in the localized state in this system, similar to the Ti doping effect for $x < 0.03$. In Ti-doped $Ca_3Ru_2O_7$, Ti impurities should act as strong scattering centers as discussed above. Under this circumstance, the electronic states from the small Fermi pockets would become incoherent due to strong impurity scattering, *i.e.* forming localized states. The increase of γ_e for these localized states may be attributed to the band structure changes caused by strong scattering. A high density of localized states near Fermi level (FL) could result in a large γ_e value. For example, the large γ_e value observed in nonstoichiometric, insulating $LaMnO_{3+\delta}$ ($\gamma_e \sim 23$ mJ/(mol K^2)) arises from the high density of localized states near the FL.[29] However, it is unclear whether the large γ_e values of our 1-2% Ti doped $Ca_3Ru_2O_7$ samples also have the similar mechanism. Clarification of this issue requires further work such as ARPES measurements.

The above discussions suggest that Ti doping significantly decreases charge carrier itinerancy despite at low doping concentration. The magnetic transition from the AFM-b to the G-AFM near $x \sim 0.03$ implies the importance of itinerant carriers in stabilizing the intrabilayer FM ordering, and this can be understood in terms of the model involving the competition between double-exchange FM and AFM super-exchange interactions. This model has been extensively studied in CMR manganites.[25] In this model, the double exchange FM interaction is mediated via the Hund's rule coupling between itinerant carriers and localized spins and a stable FM state requires sufficient itinerant carriers. In manganates, FM ordering is achieved via charge carrier doping into a Mott insulating state, while in our system, the bilayer FM ordering is tuned by charge carrier itinerancy, rather than carrier density. The incommensurate component observed near the AFM-b/AFM-a phase boundary can be ascribed to the competition between double-exchange FM and super-exchange AFM interactions. The incommensurate magnetic structure arising from competing magnetic interactions has indeed been predicted theoretically and observed in many other correlated materials.[30,31]

IV. CONCLUSION

In summary, we have conducted comprehensive studies on $Ca_3(Ru_{1-x}Ti_x)_2O_7$ via neutron scattering, resistivity, magnetization and specific heat measurements. The electronic and magnetic phase diagram of this system has been established. We found that the system can be tuned from the quasi-2D metal with the AFM-b order to the Mott-

insulating state with the G-type AFM order as x is increased above 0.05. A weakly localized state is observed for $0 < x < 0.05$ and the magnetic transition from the AFM-b to the G-AFM state is found to take place near $x = 0.03$. Such inconsistency between the electronic and magnetic transitions can be attributed to the doping-induced chemical inhomogeneity, which leads to the magnetic phase separation and the electronic percolation effect near the magnetic phase boundary. We have discussed the mechanism for such electronic and magnetic phase transitions induced by Ti doping. Our analyses show that the Mott transition induced by Ti doping is not associated with the band filling or the structural distortion, but should be attributed to the band narrowing caused by strong scattering from Ti impurities. The magnetic transition from the intralayer FM coupling to the nearest-neighbor AFM coupling near $x = 0.03$ can be understood in light of the competition between double-exchange FM and AFM super-exchange interactions. The variation of charge carrier itinerancy plays a critical role in tuning such a magnetic transition.

V. ACKNOWLEDGEMENT

This work is supported by the DOD ARO under Grant No. W911NF0910530 and the NSF under Grant DMR-1205469. Experimental work at ORNL was supported by the Scientific User Facilities Division, Office of Basic Energy Sciences, DOE. Work at NJU is supported by National Key Projects for Basic Research of China (No. 2010CB923404) and the Natural Science Foundation of China (10974081, 10979017).

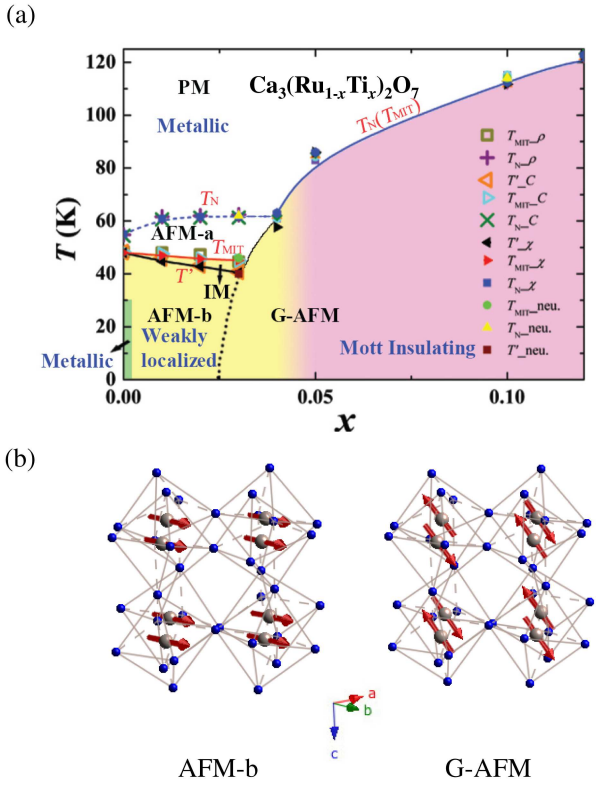

FIG. 1: (color online) (a) Magnetic and electronic phase diagram of $Ca_3(Ru_{1-x}Ti_x)_2O_7$. AFM-a/b: FM bilayers coupled antiferromagnetically along c axis with spin along the a/b axis; G-AFM: Nearest-neighbor antiferromagnetic state; IM: intermediate magnetic state; PM: paramagnetic. The phase boundaries among these various magnetic states are given by solid/dotted lines. Various colors represent different electronic states. (b) Schematics of the magnetic structures for the AFM-b and G-AFM phases.

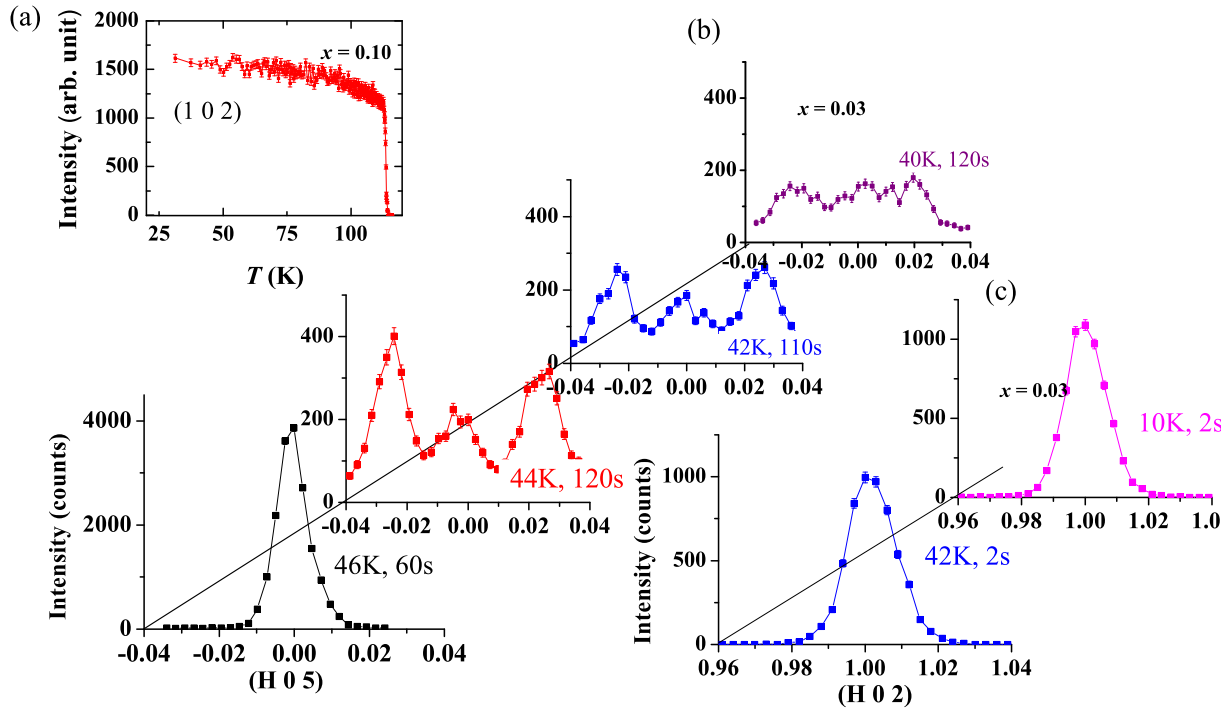

FIG. 2: (color online) (a) Temperature dependence of the magnetic Bragg peak intensity at (102) for the $x = 0.10$ sample; (b) Magnetic Bragg peaks at (005) and ($\pm\delta$, 0, 5) for the $x = 0.03$ sample, measured at various temperatures; (c) (102) magnetic Bragg peak for the $x = 0.03$ sample at $T = 42$ K, and 10 K. Note that the counting time is different for each spectrum in (b) and (c).

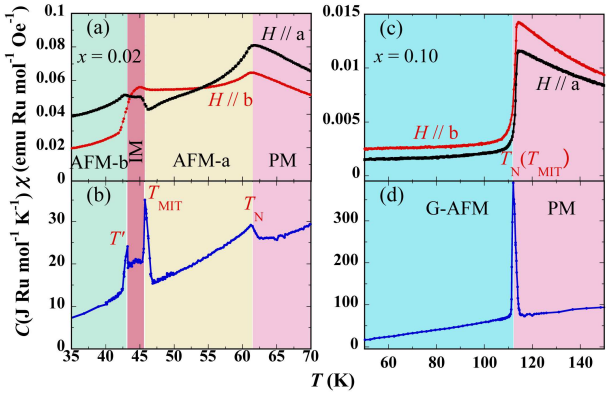

FIG. 3: (color online) Magnetic susceptibility vs. T measured under the magnetic field of 100 Oe for the $x = 0.02$ (a) and $x = 0.10$ (c) samples; Specific heat vs. T for the $x = 0.02$ (b) and $x = 0.10$ (d) samples.

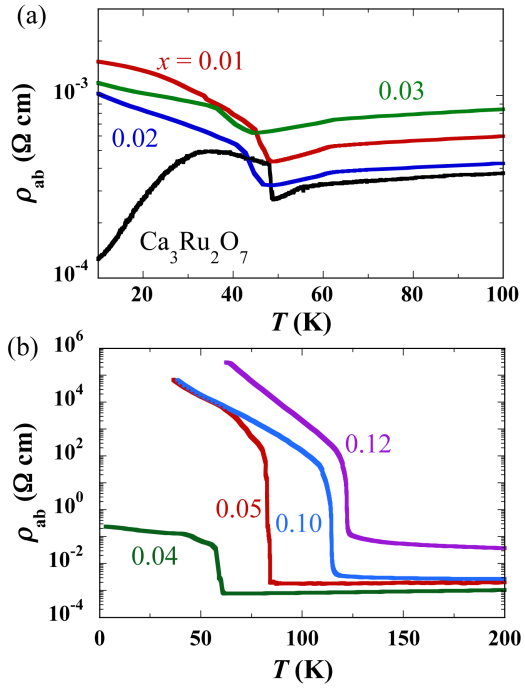

FIG. 4: (color online) In-plane resistivity as a function of temperature for various samples. The data for $x = 0$, 0.03, 0.05 and 0.1 were reported in our earlier work[24] and are included here for comparison.

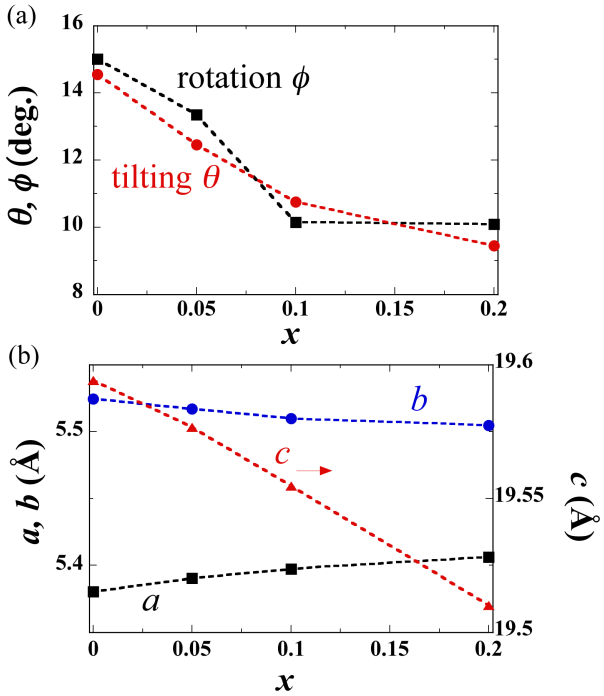

FIG. 5: (color online) (a) Rotation and tilting angles of RuO_6 octahedra as a function of Ti content; (b) Lattice parameters a, b and c as a function of Ti content.

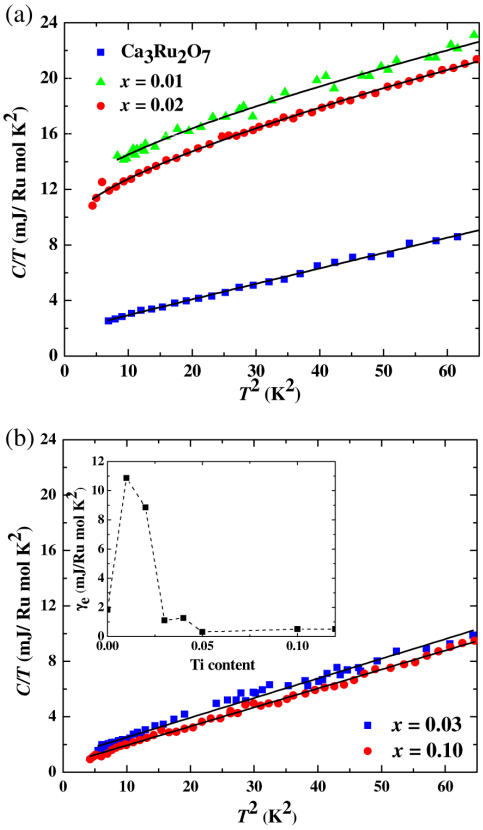

FIG. 6: (color online) Low temperature specific heat data for the samples with $x = 0$, 0.01, 0.02 (a), and $x = 0.03$, 0.10 (b). The solid lines represent fits of the data (see the text for details). Inset: Electronic specific heat coefficient as a function of Ti content.

* Electronic address: zmao@tulane.edu

[1] E. Dagotto, Science **309**, 257 (2005).
[2] S. N. Ruddlesden and P. Popper, Acta Crystallogr **10**, 538 (1957).
[3] A. P. Mackenzie and Y. Maeno, Rev. Mod. Phys. **75**, 657 (2003).
[4] K. Ishida, H. Mukuda, Y. Kitaoka, K. Asayama, Z. Q. Mao, Y. Mori, and Y. Maeno, Nature **396**, 658 (1998).
[5] K. D. Nelson, Z. Q. Mao, Y. Maeno, and Y. Liu, Science **306**, 1151 (2004).
[6] S. A. Grigera, R. S. Perry, A. J. Schofield, M. Chiao, S. R. Julian, G. G. Lonzarich, S. I. Ikeda, Y. Maeno, A. J. Millis, and A. P. Mackenzie, Science **294**, 329 (2001).
[7] S.-I. Ikeda, Y. Maeno, S. Nakatsuji, M. Kosaka, and Y. Uwatoko, Phys. Rev. B **62**, R6089 (2000).
[8] R. A. borzi, S. A. Grigera, J. Farrell, R. S. Perry, S. J. S. Lister, S. L. Lee, D. A. Tennant, Y. Maeno, and A. P. Mackenzie, Science **315**, 214 (2006).
[9] R. S. Perry, L. M. Galvin, S. A. Grigera, L. Capogna, A. J. Schofield, A. P. Mackenzie, M.Chiao, S. R. Julian, S. I. Ikeda, S. Nakatsuji, et al., Phys. Rev. Lett. **86**, 2661 (2001).
[10] L. Klein, J. S. Dodge, C. H. Ahn, G. J. Snyder, T. H. Geballe, M. R. Beasley, and A. Kapitulnik, Phys. Rev. Lett. **77**, 2774 (1996).
[11] S. Nakatsuji and Y. Maeno, Phys. Rev. Lett. **84**, 2666 (2000).
[12] S. Nakatsuji and Y. Maeno, Phys. Rev. B **62**, 6458 (2000).
[13] R. G. Moore, J. Zhang, V. B. Nascimento, R. Jin, J. Guo, G. T. Wang, Z. Fang, D. Mandrus, and E. W. Plummer, Science **318**, 615 (2007).
[14] J. Zhang, Ismail, R. G. Moore, S. C. Wang, H. Ding, R. Jin, D. Mandrus, and E. W. Plummer, Phys. Rev. Lett. **96**, 066401 (2006).
[15] G. Cao, K. Abbound, S. McCall, J. E. Crow, and R. P. Guertin, Phys. Rev. Lett. **78**, 1751 (1997).
[16] W. Bao, Z. Q. Mao, Z. Qu, and J. W. Lynn, Phys. Rev. Lett. **100**, 247203 (2008).
[17] Y. Yoshida, S.-I. Ikeda, H. Matsuhata, N. Shirakawa, and S. Katano, Phys. Rev. B **72**, 054412 (2005).
[18] Y. Yoshida, I. Nagai, S.-I. Ikeda, N. Shirakawa, M. Kosaka, and N. Mori, Phys. Rev. B **69**, 220411 (2004).
[19] J. S. Lee, S. J. Moon, B. J. Yang, J. Yu, U. Schade, Y. Yoshida, S. L. Ikeda, and T. W. Noh, Phys. Rev. Lett. **98**, 097403 (2007).
[20] H. L. Liu, S. Yoon, S. L. Cooper, G. Cao, and J. E. Crow, Phys. Rev. B **60**, R6980 (1999).
[21] F. Baumberger, N. J. C. Ingle, N. Kikugawa, M. AHossain, W. Meevasana, R. S. Perry, K. M. shen, D. H. Lu, A. Damascelli, A. Rost, et al., Phys. Rev. Lett. **96**, 107601 (2006).
[22] D. J. Singh and S. Auluck, Phys. Rev. Lett. **96**, 097203 (2006).
[23] D. Fobes, J. Peng, Z. Qu, T. J. Liu, and Z. Q. Mao, Phys. Rev. B **84**, 014406 (2011).
[24] X. Ke, J. Peng, D. J. Singh, T. Hong, W. Tian, C. R. D. Cruz, and Z. Q. Mao, Phys. Rev. B **84**, 201102 (2011).
[25] M. B. Salamon and M. Jaime, Rev. Mod. Phys. **73**, 583 (2001).
[26] B. F. Woodfield, M. L. Wilson, and J. M. Byers, Phys. Rev. Lett **78**, 3201 (1997).
[27] C. He, S. Eisenberg, C. Jan, H. Zheng, J. G. Mitchell, and C. Leighton, Phys. Rev. B **80**, 214411 (2009).
[28] Z. Qu, J. Peng, T. J. Liu, D. Fobes, L. Spinu, and Z. Q. Mao, Phys. Rev. B **80**, 115130 (2009).
[29] L. Ghivelder and I. A. Castillo, Phys. Rev. B **60**, 12184 (1999).
[30] G. Lawes, M. Kenzelmann, N. Rogado, K. H. Kim, G. A. Jorge, R. J. Cava, A. Aharony, O. Entin-Wohlman, A. B. Harris, T. Yildirim, et al., Phys. Rev. Lett. **93**, 247201 (2010).
[31] F. Ye, Y. Ren, J. A. Fernanadez-Baca, H. A. Mook, J. W. Lynn, R. P. Chaudhury, Y. Q. Wang, B. Lorenz, and C. W. Chu, Phys. Rev. B **78**, 193101 (2008).